URN

UNDERGRADUATE RESEARCH NEWSLETTER

Table of Contents

Editors

Faculty Advisor

Professor Burjor Captain
Department of Chemistry

Student Editors

Molly Bickle
Allyson Hudak
Bella Kimbel
Calvin Leung

Review Board

Students

Molly Bickle
Allyson Hudak
Bella Kimbel
Calvin Leung

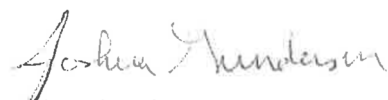*Faculty*

Burjor Captain, Chemistry

Foreword

I am very happy to be asked to contribute the Foreword to the Undergraduate Research Newsletter (URN). The URN provides an excellent forum to highlight some of the leading-edge research being conducted by undergraduates at the University of Miami (UM) and simultaneously serves as a capstone for their work. Undergraduate research opportunities complement the standard curriculum of coursework and labs in a way that ideally prepares undergraduates for real-world research experiences in future jobs that span academia, government and the private sector.

My own undergraduate research experience started a long time ago (almost 40 years!) as a second semester freshman working in MIT's Gravity Group. I joined the group because I wanted to help with an experiment to make the first detection of gravity waves; however, as it turned out, there was a more immediate need for undergraduate assistance on a project to study the intricacies of the cosmic microwave background (CMB). I continued my work in the lab for all my remaining semesters and summers at MIT - I was hooked! Not only was I hooked, but in retrospect, I was lucky that my initial interests in gravity waves were diverted into CMB studies. CMB studies were a rich area of study in the ensuing years while gravity waves took another 30 years to discover. I extended on this initial CMB work as a PhD student, postdoc and faculty member here at UM. There is a clear through line between my current research pursuits and my undergraduate research experience that underscores how formative the process can be.

The tables have turned, and now I strive to provide a similarly formative and enriching experience to UM undergrads. I have to believe that this is a common goal for all UM researchers who engage undergrads in their research. In reviewing the articles for this URN, I was struck by the quality and depth of the research work that is communicated in these articles - not to mention the breadth. Hats off to the students for all their hard work and their mentors for providing the necessary guidance and review. I sincerely hope and strongly suspect that the five author's research projects can be used as springboards to additional publications or graduate school research .

Joshua Gundersen
Professor of Physics

The Synthesis and Characterization of Novel Metformin-Glucose Carbon Dots

Jordan M. Garber (Class of 2024)
Major: Chemistry
Principal Investigator: Roger M. Leblanc
Graduate Student Co-Mentor: Emel Kirbas Cilingir
Department: Chemistry

Carbon quantum Dots (CDs) have been escalating in popularity in the past decade because they retain a select group of keen characteristics that make them a phenomenal choice in bioimaging, drug delivery, synthetic chemistry, and medicinal medicine. CDs are recognized as an exceptional nanocarriers as they are credited with high photoluminescence (PL), high photostability, excellent biocompatibility, and remarkable tunable surface functionality [1] . Traditional quantum dots deviate from CDs since CDs are environmentally friendly, nontoxic, and inexpensive to produce, triggering swift advancements of CDs as a nanomaterial [1] . CDs are classified as a dimensionless nanoparticle with a diameter less than 10 nm across and a crystal lattice parameter of 0.34 nm [1,2,3] . Generally, there are two widely accepted approaches to synthesizing CDs: (1) top-down approach and (2) bottom-up approach. The top-down approach degrades a pure carbon source into a powder then into ultra-small compounds [4]. In the top-down approach, a chemical, electrochemical, electrolysis, acid, reflux, or laser ablation can be used to degrade the carbon source into CDs [5]. The bottom-up approach utilizes small, organic, precursor molecules and ionizes them to form ions, radicals, and electrons which condenses into aromatic clusters of CDs [5]. As scientists started to incorporate a variety of organic compounds as a procurer, CDs can exhibit numerous of different properties which are intended for applicable research purposes [6,7]. Some studies' results indicate that some of the precursor molecule can incorporate itself as a surface functional group, allowing the original precursor to preserve its original functionality.

This study focuses and introduces the synthesis of metformin-glucose carbon dots, abbreviated Met-G CDs, a novel CD, for the first time in the published literature.

We have designed a protocol for a bottom-up approach for Met-G-CDs by using microwave-assisted method. Both metformin and glucose are used as the organic precursor. Metformin is a generic prescription drug that is primary used to treat Type 2 Diabetes Mellitus [8,9]. Metformin recently was proved to improve insulin resistance by impeding gluconeogenesis; consequently, decreasing blood sugar levels [10]. Metformin, specifically, activates AMP protein kinases (AMPK) to phosphorylate CREB binding proteins, inhibiting gluconeogenesis which downregulates glucose production, allowing skeletal muscle to absorb more sugar. Current literature explains that metformin accumulates in mitochondria at a concentration that is 100-fold more concentrated than in the cytosol [8]. Metformin is forced into the mitochondrial matrix because of its positively surface charge However, because metformin regulates natural insulin production, it can also be used as a chemotherapeutic to inhibit cancer growth [9]. As expressed previously, despite metformin being a precursor, it is expected for it to be incorporated as a surface group, expecting the carbon dot to also accumulate in the matrix. Mitochondrial localization can be imperative for any nanocarrier since mitochondria impact cellular metabolism (ex. ATP production, storage of Ca2+, and regulating apoptosis). Considering how mitochondrial storage and clinical diseases such as Alzheimer's, Parkinson's, Alper's, or Leigh disease are directly related to mitochondrial physiology, regulating mitochondrial metabolism and behavior is vital and possible with CDs [10]. Glucose is the second organic precursor that is used to establish both itself and carboxylic groups as surface structure. The use of glucose as a pharmaceutical as opposed to a nutritional agent is gaining recent attention after the discovery that cancer consumes large amounts of sugar [11]. As GLUT-1 is the transport protein responsible for glucose uptake, it is overexpressed in cancerous tissues, especially liver and renal cancers [12] . Glucose-based pharmaceuticals were first developed in 1995 with the creation of glufosfamide which is partially GLUT-receptor mediated [12]. In this this study, both metformin and glucose were used as organic precursors and were extensively characterized with Fourier Transform Infrared spectroscopy (FTIR), ultra-violet spectroscopy (UV-Vis) photoluminescence (PL), atomic force (AFM), X-ray photoelectron spectroscopy (XPS), and transmission electron (TEM) microscopies. Spectroscopic results demonstrate strong

results for anticancer therapeutics with high expression of surface carboxylic groups and positive surface charge.

Met-G-CDs were synthesized utilizing a microwave-mediated approach. 250 mg of metformin • HCl (MW = 163.63 g/mol) and 275 mg or dextrose (MW = 180.16 g/mol) was dissolved in 25 mL of water; metformin hydrochloride (purity > 99%) was obtained from MP Biomedicals (Irvine, CA). The solution needs to be stirred for approximately 30 minutes before it is microwaved in a standard domestic microwave for 5 minutes at 700W to emit a total of 210 kJ. A brown and black residue should be collected and dispensed in 15 mL of water in the container. The new solution should undergo sonication for 30 minutes. After sonication, it is centrifuged for 30 minutes at 9,000 RPM at 21°C. The supernatant is extracted and filtered through a 0.2 mm filter membrane (VWR, US). The filtrate underwent dialysis in 100-500 Da MWCO dialysis tubbing for three days in DI water, replacing the water every day. The sample was placed into a freezer at -40C for 24 hours, and then finally went lyophilization for 4 days using a FreeZone for a 4.5L cascade benchtop freeze dry system. The solvent of choice was DI water which was purified using a MilliQ3 water purification system obtained from Millipore Sigma (Burlington, MA). The surface tension of the purified deionized water is 72.6 mN_m_1 with a resistivity of 18 MX_cm and a pH of 6.6 ± 0.3 at 20.0 ± 0.5 _C. The dialysis bags were Spectrapor dialysis tubing with a molecular weight cutoff (MWCO) of 100-500 Da was purchased from VWR (West Chester, PA).

Met-G CDs (conc.) was initially characterized using solid Perkin Elmer FTIR (Frontier, US) spectroscopy fitted with an ATR prism for baseline scans in the hope to identify optimal and keen surface functional groups. To approximate and determine the molecular mass of Met-G CDs, Matrix-Assisted Laser Desorption/Ionization Time of Flight (MALDI-TOF) mass spectrometry (MS) was executed by utilizing a Bruker auto flex speed spectrometer. Met-G CDs underwent further characterization with UV-vis absorption spectroscopy. Met-G CDs were dissolved in an aqueous medium in 1x1 cm quartz cell (Strana Cells, Inc; Atascadero, CA) with a Cary 100 UV-vis spectrometer (Agilent Technologies, USA). Met-G CDs, conversely, underwent further characterization in an aqueous medium by acquiring a florescence emission spectrum by utilizing a Horiba Jobin Yvon Fluorolog-3 with a slit width of 5 nm

for both excitation and emission. The surface charge of Met-G CDs was obtained by determining the zeta potential. A DLS nano series Malvern Zetasizer (Westborough, MA) was exploited to gain the zeta potential.

Met-G CDs' fluoresce quantum yield (Φ) was deduced by contrasting the integrated area of the fluoresce curve and absorbance intensity values against standards. Quinine sulfate, harmane, and lucigenin were the chosen standards with known fluoresce quantum yield values of 54%, 83%, 65% respectively [13]. As Quinine sulfate and harmane were dissolved in H2SO4 with a known refractive index (Rn) of 1.33 at 350 nm, lucigenin and Met-G CDs were dissolved in water with a known refractive index (Rn) of 1.33 at 350 nm [13]. After obtaining the fluoresce spectra, UV-vis absorbance was measured at 350 nm and assuring that the absorbance intensity was below 5%. The mean quantum yield (Φ) was achieved by computing the quantum yield (Φ) against each standard using:

$$\Phi = \Phi_r \times \frac{I}{I_R} \times \frac{A_R}{A} \times \left(\frac{n_R}{n}\right)^2$$

where Φ_R, I, A, n represent the literature quantum yield of a standard, integrated area under the fluoresce curve, the absorbance intensity at 350 nm, and the refractive index respectively; R is designated for values of the standards.

Met-G CDs surface carboxylic groups were approximated by assembling and utilizing a gravimetric titration with a pH probe tracking the acidity of aqueous Met-G CDs. It is assumed that the carbon dots behave as a strong acid, so when titrated against a strong base, the concertation of protons is easily measured at the pH of 7. A milligram of Met-G CDs was dissolved in water and titrated with 0.01M NaOH. Sine the amount of hydroxide ions added equals the number of protons, the amount of hydroxide added is equivalent to the number of surface carboxylic groups.

Met-G CDs synthesis was manicured to yield a pure product as expressed above. The most critical and important step in the synthesis of any carbon dot is purification of impurities as any excess reactants and fluorophores obstructs optical properties and biocompatibility [13]. Considering the applications Met-G CDs pose, three distinct methods were enacted into the protocol to ensure a purified sample: (1) centrifugation, (2) syringe filtration,

and (3) dialysis. A proposed mechanism of polymerization was hypothesized based on former research conducted. The polymerization, condensation reaction is believed to begin when the carbonyl group of an aldehyde of glucose reacts with a primary amine of metformin in an imine formation. With additional energy, the heat stabilizes the imine to allow for the formation of Met-G CDs because of the creation of carbonizations. UV-vis spectroscopy indicated an absorption band (λmax) at 350 nm which is a common characteristic of nitrogen doped carbon dots as bands between 300-450nm are n-π* electronic transition of both amines and imines [14, 15, 16].
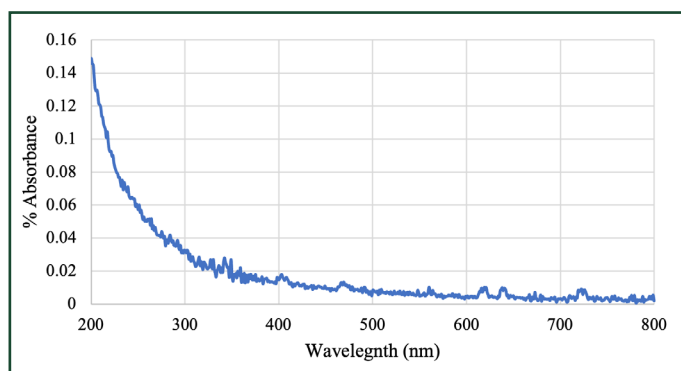

Figure 2. FTIR Spectra of Met-G CDs

Figure 1. UV-vis Spectra of Met-G CDs

FTIR spectroscopy with an ATR accessory was exercised to identify surface functional groups. Carboxylic acids (peaks at 3200 cm-1 and 1745 cm-1) and amine (peaks at 3314 cm-1, 1209 cm-1, and 1048 cm-1) were distinguished on the surface of Met-G CDs. Both O-H and N-H stretching was identified at peaks 3200 cm-1 and 3314 cm-1 respectively. While the peak at 2928 cm-1 is attributed to C-H stretching, the band at 2148 cm-1 resembles C≡C stretching. The other distinguished peaks at 1572 cm-1, 1404 cm-1, 1300 cm-1, 1048 cm-1, and 886 cm-1 correspond to N-O stretching, O-H bending, O-H bending, N-O bending, and N-H dimers respectively. As it is important to note that neither percussors contained N-O bonds, it was confirmed to be on the surface of Met-G CDs.

After the surface of Met-G CDs were characterized, the zeta potential was found to be 21.4 mV.

Both the broad N-H stretching at 3314 cm-1 the positive surface charge, consequently, confirms the hypothesis of imine formation. Considering carbon dots have inherited
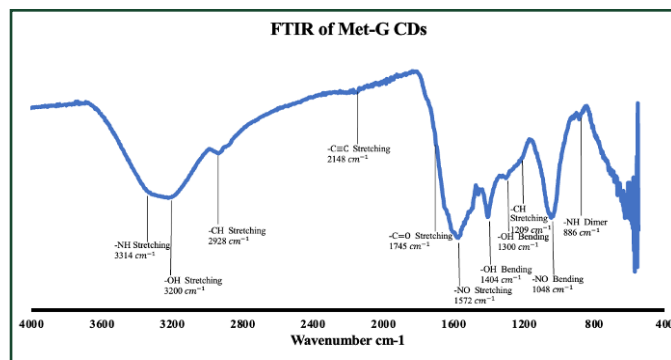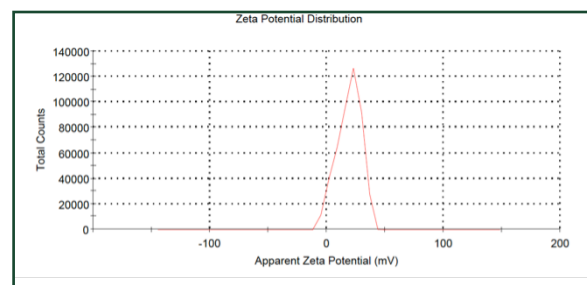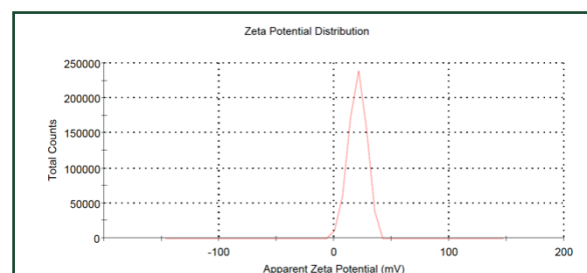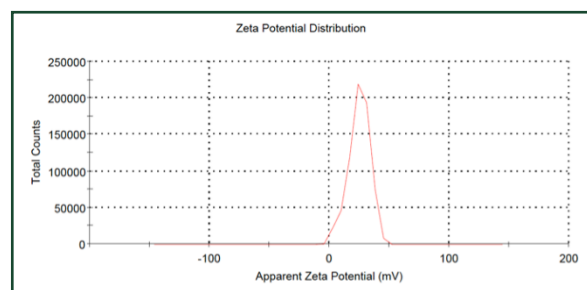

Figure 3. Zeta Potential Distribution of Met-G CDs

properties of being good bioimagers, biomarkers, and biosensors, the fluorescence quantum yield (QY) is especially critical because it relays the brightness of a nanoparticle. Since QY calculations involves various, unswerving protocols and apparatus, it is imperative to select two references. References being a highly
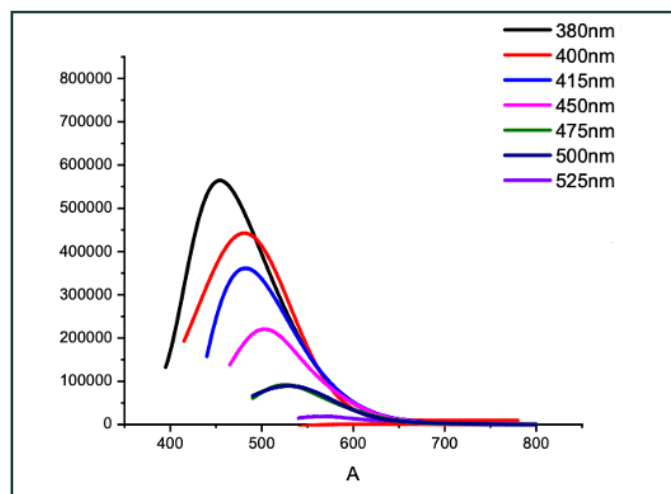
Figure 4. Fluorescence Spectra of Met-G CDs

Figure 5. MALDI-MS of Met-G CDs

researched and highly characterized substances with an accepted and established QY. The use of two references allows for cross-calibration, minimizing the effect of outlying data. The excitation wavelength and an emission range for both Met-G CDs and the references were 350 nm and 400-600 nm respectively because it aligns with literature ranges of the references.

As expressed before, the use of several references allows for cross calibration; therefore, in this study, two were used to further the accuracy and validity of the results. The chosen references were Quinine sulfate and Harmane with computed QY of 98% and 45% respectively. With the confirmation of precise, calculated QY values of the references within ±19%, Met-G CDs were dissolved in DI water to discover its QY. Using the same protocol for the references, the fluorescence quantum yield was calculated at 3.79%. MALDI-TOF, a form of mass spectroscopy, affirms that Met-G CDs have a M+ peak at 454.513 g/mol.

Met-G CDs are also characterized to have a relative high number of carboxylic groups with 0.005 mmol on the surface of the carbon dots with a pH of 7.00 after the addition of 0.5 mL of 0.01M NaOH.

Since the combination of both glucose and metformin have never been percussors to yield a carbon-based nanoparticle, Met-G CDs are original, novel, and first of its kind. After decisive purification, Met-G CDs were extensively and comprehensively characterized using several techniques: (1) UV-vis, (2) FTIR, (3), PL, (4)
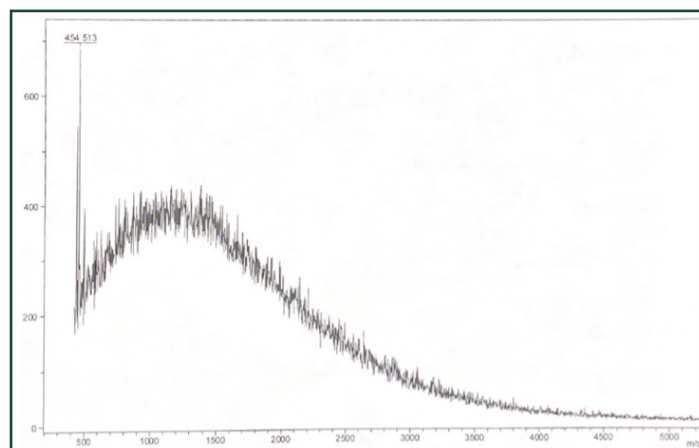
MALDI-MS, and (5) zeta potential. With the vast array of results of characterizations, Met-G CDs exhibit great potential as a drug delivery mechanism for cellular targeting with high tuneability using nanoarchitectonics and drug conjugation. While only preliminary studies have been conducted on the cell viability of Met-G CDs, the results are promising, asserting Met-G CDs are a viable candidate as a chemotherapeutic. More studies are still being investigated with the conjugation of Met-G CDs with idarubicin through an EDC/NHS coupling mechanism. While it is too early to report exact figures, Met-G CDs appear to be an excellent candite as a nanocarrier.

References

[1] Zheng, X. T.; Ananthanarayanan, A.; Luo, K. Q.; Chen, P. Glowing Graphene Quantum Dots and Carbon Dots: Properties, Syntheses, and Biological Applications. Small (Weinheim an der Bergstrasse, Germany) 2015, 11, 1620-1636.

[2] Fernando, K. A. S.; Sahu, S.; Liu, Y.; Lewis, W. K.; Guliants, E. A.; Jafariyan, A.; Wang, P.; Bunker, C. E.; Sun, Y. Carbon Quantum Dots and Applications in Photocatalytic Energy Conversion. ACS applied materials & interfaces 1900, 7, 8363-8376.

[3] Ding, C.; Zhu, A.; Tian, Y. Functional Surface Engineering of C Dots for Fluorescent Biosensing and in Vivo Bioimaging. Accounts of chemical research 2014, 47, 20-30.

[4] Iravani, S.; Varma, R. S. Green synthesis, biomedical and biotechnological applications of carbon and graphene quantum dots. A review. Environ Chem Lett 2020, 18, 703-727.

[5] Zheng, X. T.; Ananthanarayanan, A.; Luo, K. Q.; Chen, P.

Glowing Graphene Quantum Dots and Carbon Dots: Properties, Syntheses, and Biological Applications. Small (Weinheim an der Bergstrasse, Germany) 2015, 11, 1620-1636.

[6] Mehta, V. N.; Jha, S.; Basu, H.; Singhal, R. K.; Kailasa, S. K. One-step hydrothermal approach to fabricate carbon dots from apple juice for imaging of mycobacterium and fungal cells. Sensors and actuators. B, Chemical 2015, 213, 434-443.

[7] Hettiarachchi, S. D.; Graham, R. M.; Mintz, K. J.; Zhou, Y.; Vanni, S.; Peng, Z.; Leblanc, R. M. Triple conjugated carbon dots as a nano-drug delivery model for glioblastoma brain tumors. Nanoscale 2019, 11, 6192-6205.

[8] Hundal, R. S.; Inzucchi, S. E. Metformin: New Understandings, New Uses. Drugs (New York, N.Y.) 2003, 63, 1879-1894.

[9] Dowling, R. J. O.; Niraula, S.; Stambolic, V.; Goodwin, P. J. Metformin in cancer: translational challenges. Journal of molecular endocrinology 2012, 48, R31-R43.

[10] Hua, X.; Bao, Y.; Chen, Z.; Wu, F. Carbon quantum dots with intrinsic mitochondrial targeting ability for mitochondria-based theranostics. Nanoscale 2017, 9, 10948-10960.

[11] Warburg, O.; Wind, F.; Negelein, E. THE METABOLISM OF TUMORS IN THE BODY. The Journal of General Physiology 1927, 8, 519-530.

[12] Calvaresi, E. C.; Hergenrother, P. J. Glucose conjugation for the specific targeting and treatment of cancer. Chemical science (Cambridge) 2013, 4, 2319-2333.

[13] Kirbas Cilingir, E.; Seven, E. S.; Zhou, Y.; Walters, B. M.; Mintz, K. J.; Pandey, R. R.; Wikramanayake, A. H.; Chusuei, C. C.; Vanni, S.; Graham, R. M.; Leblanc, R. M. Metformin derived carbon dots: Highly biocompatible fluorescent nanomaterials as mitochondrial targeting and blood-brain barrier penetrating biomarkers. Journal of colloid and interface science 2021, 592, 485-497.

[14] Liyanage, P. Y.; Graham, R. M.; Pandey, R. R.; Chusuei, C. C.; Mintz, K. J.; Zhou, Y.; Harper, J. K.; Wu, W.; Wikramanayake, A. H.; Vanni, S.; Leblanc, R. M. Carbon Nitride Dots: A Selective Bioimaging Nanomaterial. Bioconjugate chemistry 2019, 30, 111-123.

[15] Liu, S.; Tian, J.; Wang, L.; Luo, Y.; Sun, X. A general strategy for the production of photoluminescent carbon nitride dots from organic amines and their application as novel peroxidase-like catalysts for colorimetric detection of H2O2 and glucose. RSC advances 2012, 2, 411-413.

[16] van Dam, B.; Nie, H.; Ju, B.; Marino, E.; Paulusse, J. M. J.; Schall, P.; Li, M.; Dohnalová, K. Carbon Dots: Excitation+Dependent Photoluminescence from Single-Carbon Dots (Small 48/2017). Small (Weinheim an der Bergstrasse, Germany) 2017, 13, 1770251-n/a.

Executive Function Across Cognitive and Affective Domains: Flexibility

Grace Garvalia (Class of 2027)
Major: Neuroscience
Principal Investigator: Jennifer C. Britton, Ph.D.
Graduate Student Co-Mentor: Stephanie (Novotny) Whitney, M.S.
Department: Psychology

The ability to exert flexibility across a variety of contexts is crucial in everyday life. Flexibility in non-emotional and emotional domains may be distinct processes [1], as research indicates that affective flexibility is more predictive of psychological functioning and anxiety symptoms than cognitive flexibility [1]. Furthermore, affective flexibility research concentrates on examining how individuals switch between emotional and cognitive tasks [1, 2, 3]. Our group has begun to research how individuals switch between negative and positive emotions (i.e., valence flexibility) [4, 5]. The purpose of this ongoing study is to examine flexibility in non-emotional and emotional contexts using task-based switching. To date, undergraduate students (n=255) completed tasks assessing cognitive, affective, and valence flexibility as well as additional tasks that assess other executive functions (e.g., working memory, response inhibition). Although data collection is ongoing and comprehensive statistical analyses have not yet been conducted, results from this research may highlight the importance of understanding unique contributions of cognitive, affective, and valence flexibility to psychopathology and their potential relevance for tailored interventions aimed at improving psychological well-being.

Executive function skills are a set of cognitive processes (e.g., attention control, working memory, response inhibition, flexibility) that regulate behavior to achieve goals [6] and are crucial for everyday life. Among these skills, cognitive flexibility is a fundamental ability enabling individuals to adjust in response to shifting environmental demands [7]. For example, cognitive flexibility is demonstrated when someone seamlessly transitions from solving a mathematical problem to engaging in a creative writing exercise, showcasing their ability to adapt their thinking across different domains.

In daily functioning and interpersonal interactions, individuals must be flexible not only cognitively, but also across emotional experiences [8]. For example, failure to exhibit flexibility can result in difficulty disengaging from negative emotional stimuli and shifting towards more positive stimuli [2, 9, 10], which has been linked to psychological dysfunction, particularly the tendency for rumination following negative events in daily life [11].

Experimental investigations of flexibility predominantly utilize instructed task-switching paradigms, wherein participants are prompted by a cue to alternate between task rules. For example, the Dimension Change Card Sort (DCCS) task measures one's ability to switch from identifying an item that matches by shape to identifying an item that matches by color [12]. This cognitive operation (i.e., switching) requires the inhibition of previous task rules while activating new ones, resulting in higher cognitive demands compared to task repetition [13]. These increased cognitive demands are reflected in performance deficits, commonly referred to as 'switch costs' measured by reduced accuracy and prolonged response times [14]. Elevated switch costs, signaling cognitive inflexibility, are often noted among individuals with psychiatric disorders like anxiety and depression, potentially exacerbating the presentation of typical psychopathological symptoms [15].

While traditional assessments have focused on cognitive flexibility using non-affective stimuli, affective flexibility— the ability to adapt responses to emotionally salient stimuli—has gained attention in recent research [1, 2, 9]. Recent research has begun to examine differences between cognitive and affective flexibility at both the brain and behavioral levels. [1, 2, 9]. While emerging evidence suggests separate brain-based mechanisms for processing affective and cognitive stimuli [16], empirical investigations of cognitive flexibility and affective flexibility have yielded mixed findings, with some studies indicating a significant difference while others reporting negligible or no significant difference between the operationalized measured variable (i.e., the mean RT 'switch cost') for each respective domain [9, 10, 11]. Our group has preliminary evidence that flexibility within the cognitive domain and flexibility between cognitive and affective domains may be distinct [1, 5].

In addition to these distinctions, the ability to switch

between emotional states, known as valence flexibility, may also play a crucial role in optimal mental health. Research indicates that the capacity to flexibly switch between emotional valences (e.g., switching from negative to positive emotional states) may be necessary for optimal emotion regulation [17], yet this concept has largely been overlooked in the literature. Thus, our group has recently developed a body of research examining valence flexibility in relation to cognitive or affective flexibility and psychopathology symptoms [1, 4, 5, 17]. For example, using a verbal generation task, we found that flexibility in the emotional domain was more associated with several measures of psychological functioning and anxiety symptoms, after controlling for cognitive flexibility [1]. However, no studies have compared cognitive flexibility, affective flexibility, and valence flexibility. The ongoing study described here is aimed at addressing this gap in literature.

Undergraduate students from the University of Miami reported internalizing symptoms as well as cognitive and emotional function via a Qualtrics survey. Additionally, participants completed a total of fourteen different tasks to assess flexibility as well as other executive functions (e.g., working memory and response inhibition) across the non-emotional, non-emotional/emotional, and emotional domains in randomized order. In all flexibility tasks, the trials were classified based on whether the task changed from the previous trial (i.e., switch trial) or remained the same (i.e., non-switch/repeat trial). Switch cost was then calculated as the difference in average reaction time between accurate switch and non-switch/repeat trials. Smaller switch costs indicate flexibility, whereas larger switch costs indicate inflexibility.

The Dimensional Change Card Sort Task (DCCS) was administered on an iPad as part of a battery from the National Institutes of Health (NIH) Toolbox [18]. During the DCCS task (Figure 1), participants viewed a gold star to draw their attention to the middle of the screen. A word cue (i.e., shape or color) appeared indicating the matching rule for that trial. Then, a colored shape (e.g., white boat) appeared in the middle of the screen, with two response options below the target image (e.g., white rabbit, brown boat). For the shape condition, participants were asked to select the object that matched the shape of the target (e.g., brown boat) via touchscreen. For the color condition, participants were asked to select the object that matched

the color of the target (e.g., white rabbit). For each trial, participants selected the object via touchscreen and then returned their index finger to a home base. The trial did not advance until a response was given.
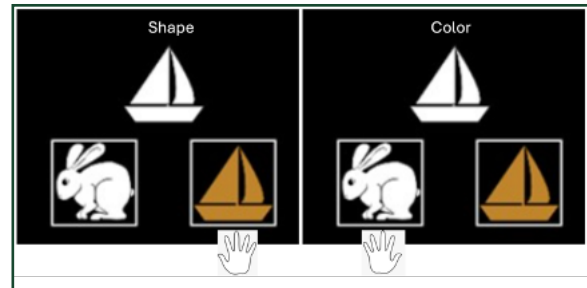

Figure 1: An example of the participant's practice trial for the shape (left) and color (right) conditions.

In this E-Prime 2.0-programmed task [19], participants viewed a word cue (i.e., gender or emotion) under a facial expression (Figure 2). Fearful and happy expressions of four female and four male faces from the NIM Stim set were presented [20]. An equal number of switch and non-switch trials were presented. Via mouse button, participants responded to the cue (i.e., gender: female/male, or emotion: fearful/happy). The cue and button press designations remained on the bottom of the screen throughout the task. Participants were prompted to respond as quickly as they could without making mistakes.
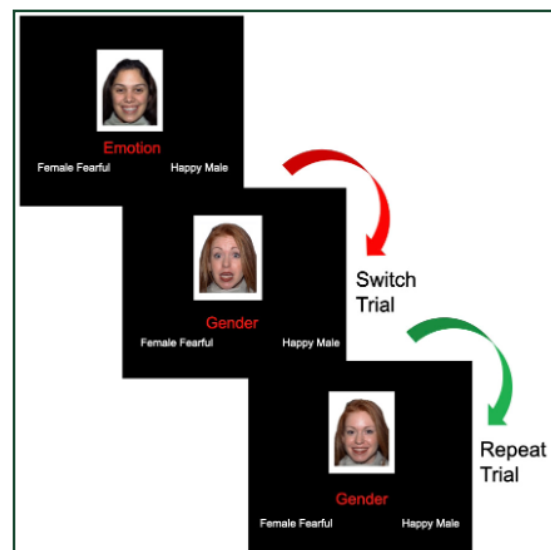

Figure 2: Examples of gender and emotion trials are displayed as well as switch and non-switch/repeat trials.

In this E-Prime 2.0-programmed task [19], participants viewed a word cue (i.e., happy or angry) in the middle of two different facial expressions of the same individual (Figure 3). Happy and angry expressions of 24 female and 24 male faces from the NIM/Radiate Stim set were presented [20, 21]. Via mouse button, participants indicated the expression that matched the word cue. Participants were prompted to respond as quickly as they could without making mistakes.
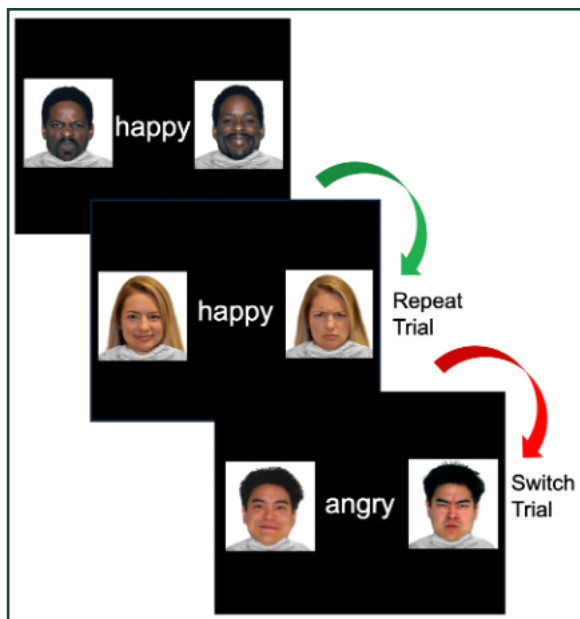

Figure 3: Valence Flexibility task.

Overall, significant differences between RT switch costs are expected across tasks. Additionally, task differences will be related to individual differences in psychopathology, such that individuals with greater anxiety symptoms will exhibit different switch cost profiles across these tasks. For example, individuals with higher levels of anxiety symptoms are expected to have more difficulty switching away from negative information towards cognitive (affective flexibility) and/or towards positive (valence flexibility) information than individuals with lower anxiety symptoms.

The primary goal of the study is to characterize cognitive and emotional differences in executive functions. Here, we focus on one aspect of this question: the relationship between cognitive, affective, and valence flexibility using commonly administered and novel tasks. Previous research suggests that cognitive and affective processes constitute separate neurobiological circuits [7, 8, 9, 16]. Therefore, greater switch costs may indicate greater cognitive resources and attentional control are needed to inhibit the processing of salient information (e.g., negative information) and to transition towards other tasks [22, 23, 24], especially in individuals with psychopathology (e.g., anxiety disorders). Identifying inflexibility when transitioning from affective to cognitive tasks or when switching between valences may help tailor interventions to improve individuals' overall executive function within emotional situations and reduce symptoms (e.g., rumination and inflexibility). Additionally, neuroimaging research has shown distinct activation patterns in other domains of executive function. For example, dorsal and rostral anterior cingulate are differentially recruited during response inhibition in cognitive and emotional contexts [25]. Therefore, future studies should also investigate the neural underpinnings of the predicted differences between cognitive, affective and valence flexibility to more fully understand the role that difficulties with flexibility contribute to the development and maintenance of psychopathology.

Acknowledgements

References

[1] Novotny, S.E., Heaney, B., Zaman, S. Benoliel, S., Ceccarelli, A., Hoffman, E., Meyyappaan, A., Snipes, A. D., & Britton, J.C. (2023, April). Ready Go! Cognitive and Emotional Item Generation, Task Constraints and Symptoms. Poster presented at Anxiety and Depression Association of America Annual Meeting, Washington, D.C.

[2] Reeck, C., & Egner, T. (2014). Emotional task management: Neural correlates of switching between affective and non-affective task-sets. Social Cognitive and Affective Neuroscience, 10(8), 1045–1053.

[3] Kraft, D., et al. 2020 Cognitive, Affective, and Feedback-Based Flexibility – Disentangling Shared and Different Aspects of Three Facets of Psychological Flexibility. Journal of Cognition, 3(1): 21, pp. 1–20.

[4] Britton, J.C., Yepes, B.E., Burdette, E.T., & Novotny,

S.E.. Development of neural correlates of valence flexibility in emotional appraisal of self and others before and after COVID-19. Manuscript in preparation.

[5] Novotny, S.E., Yepes, B.E., Burdette, E.T., & Britton, J.C. (2021). Development of Valence Flexibility Across Emotional Tasks: An fMRI study. Poster presented at American College of Neuropsychopharmacology, Virtual.

[6] Baggetta, P., & Alexander, P. A. (2016). Conceptualization and operationalization of executive function. Mind, Brain, and Education, 10(1), 10–33.

[7] Mikels, J. A., Reuter-Lorenz, P. A., Beyer, J. A., & Fredrickson, B. L. (2008). Emotion and working memory: Evidence for domain-specific processes for affective maintenance. Emotion, 8(2), 256–266.

[8] Pessoa, L. (2008). On the relationship between emotion and cognition. Nature Reviews Neuroscience, 9(2), 148–158.

[9] Genet, J. J., & Siemer, M. (2011). Flexible control in processing affective and non-affective material predicts individual differences in trait resilience. Cognition & Emotion, 25(2), 380–388.

[10] Malooly, A. M., Genet, J. J., & Siemer, M. (2013). Individual differences in reappraisal effectiveness: The role of affective flexibility. Emotion, 13(2), 302–313.

[11] Genet, J. J., Malooly, A. M., & Siemer, M. (2013). Flexibility is not always adaptive: Affective flexibility and inflexibility predict rumination use in everyday life. Cognition & Emotion, 27(4), 685–695.

[12] Doebel, S., & Zelazo, P. D. (2015). A meta-analysis of the Dimensional Change Card Sort: Implications for developmental theories and the measurement of executive function in children. Developmental Review, 38, 241–268.

[13] Vandierendonck, A., Liefooghe, B., & Verbruggen, F. (2010). Task switching: Interplay of reconfiguration and interference control. Psychological Bulletin, 136(4), 601–626.

[14] Rogers, R. D., & Monsell, S. (1995). Costs of a predictible switch between simple cognitive tasks. Journal of Experimental Psychology: General, 124(2), 207–231.

[15] Stange, J. P., Alloy, L. B., & Fresco, D. M. (2017). Inflexibility as a vulnerability to depression: A systematic qualitative review. Clinical Psychology: Science and Practice, 24(3), 245–276.

[16] Phelps, E. A. (2006). Emotion and cognition: Insights from studies of the human amygdala. Annual Review of Psychology, 57(1), 27-53.

[17] Whitney, S.E., Burdette, E.T., Yepes, B.E., & Britton, J.C. Development of neural correlates of valence flexibility in emotional experience. Manuscript in preparation.

[18] Weintraub, S., Dikmen, S. S., Heaton, R. K., Tulsky, D. S., Zelazo, P. D., Bauer, P. J., Carlozzi, N. E., Slotkin, J., Blitz, D., Wallner-Allen, K., Fox, N. A., Beaumont, J. L., Mungas, D., Nowinski, C. J., Richler, J., Deocampo, J. A., Anderson, J. E., Manly, J. J., Borosh, B., … Gershon, R. C. (2013). Cognition Assessment using the NIH toolbox. Neurology, 80(11_supplement_3).

[19] Schneider, W., Eschman, A., & Zuccolotto, A. (2002). E-Prime (Version 2.0). [Computer software and manual]. Pittsburgh, PA: Psychology Software Tools Inc.

[20] Tottenham, N., Tanaka, J. W., Leon, A. C., McCarry, T., Nurse, M., Hare, T. A., Marcus, D. J., Westerlund, A., Casey, B., & Nelson, C. (2009b). The NIMSTIM set of facial expressions: Judgments from untrained research participants. Psychiatry Research, 168(3), 242–249.

[21] Conley, M. I., Dellarco, D. V., Rubien-Thomas, E., Cohen, A. O., Cervera, A., Tottenham, N., & Casey, B. (2018). The racially diverse affective expression (radiate) face stimulus set. Psychiatry Research, 270, 1059–1067.

[22] Fox, E., Russo, R., Bowles, R., & Dutton, K. (2001). Do threatening stimuli draw or hold visual attention in subclinical anxiety? Journal of Experimental Psychology: General, 130(4), 681–700.

[23] Fox, E., Russo, R., & Dutton, K. (2002). Attentional bias for threat: Evidence for delayed disengagement from emotional faces. Cognition & Emotion, 16(3), 355–379.

[24] Mogg, K., Holmes, A., Garner, M., & Bradley, B. P. (2008). Effects of threat cues on attentional shifting, disengagement and response slowing in anxious individuals. Behaviour Research and Therapy, 46(5), 656–667.

[25] Bush, G., Luu, P., & Posner, M. I. (2000). Cognitive and emotional influences in anterior cingulate cortex. Trends in cognitive sciences, 4(6), 215–222.

Evaluation of Biological Collection Efficiency of a Bioaerosol Sampler-VIVAS

Haley Gross (Class of 2025)
Major: Microbiology and Immunology
Principal Investigator: Dr. Chang-Yu Wu
Department: Chemical, Environmental and Materials Engineering

Figure 1. Diagram of VIVAS bioaerosol samplers connected in series.

The effectiveness of bioaerosol samplers, including The Viable Virus Aerosol Sampler (VIVAS), is critical in assessing their capability to capture aerosolized infectious disease agents. VIVAS enhances our ability to capture virus particles, but a comprehensive understanding of its biological collection efficiency is lacking. To assess VIVAS biological efficiency, we introduce a novel approach to address this challenge by connecting two VIVAS samplers in series (Fig. 1).

The VIVAS utilizes a condensational growth mechanism, involving the condensation of water vapor onto particles. The mechanism leads to the enlargement and capture of fine particles containing viruses. This reduces the potential for viability losses of viruses during collection compared to impinger or filter-based methods. The growth tube collector (GTC) mechanism has a demonstrated physical collection efficiency (PCE) >90%; however, its biological collection efficiency (BCE) is unknown [1, 2]. Such a serial sampling system allows the determination of viable virus concentration at the inlet of the samplers. Comparing the viable virus collection of the first sampler with the second one enables determination of absolute biological collection efficiency of VIVAS. In this study, aerosols are produced at 4 Lpm and dried with 16 Lpm of air and collected at 8.5 Lpm through both VIVAS. Samples are assessed for viable counts using plaque assay and RT-qPCR. Preliminary results show VIVAS to be >99% biologically efficient across sampling durations of 10, 20, and 30 minutes, with no significant differences (p > 0.05) for an inlet aerosol concentration of 6-9×104 #/cc. The next phase of the study is to test its biological efficiency as a function of low and high aerosol concentrations. This data-driven approach facilitates informed decision-making regarding sampling protocols and experimental design, ultimately improving our understanding of VIVAS in capturing viable viruses.
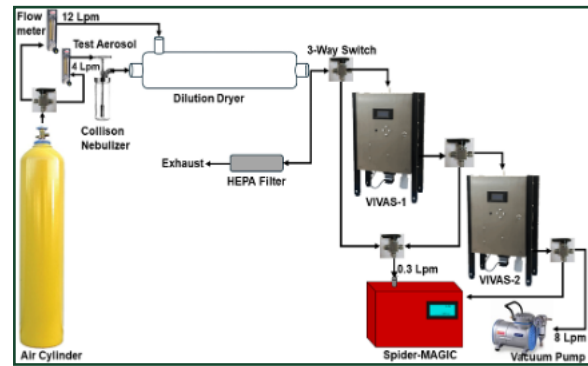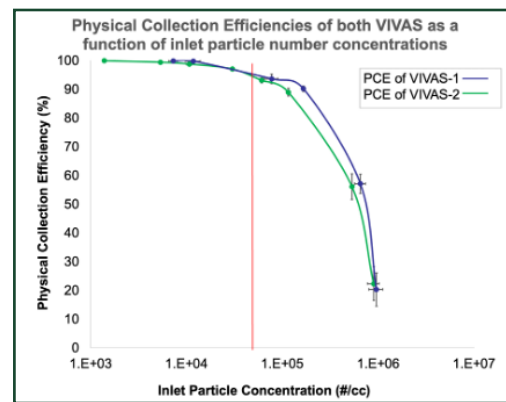

Figure 2. Shows >95% for an inlet aerosol concentration as high as 5x104 #/cc for determining BCE with varied sampling durations [1, 3].

VIVAS BCE is assessed by connecting two VIVAS samplers in series allowing the determination of viable virus concentration at both samplers' inlet (Fig. 1). PCE is used to determine the sampling conditions where VIVAS-1 and VIVAS-2 in a series have similar PCE. BCE is used to sample MS2 to determine the real BCE as a function of the Inlet particle concentration and sampling duration. This is done by calculating the plaque forming unit (PFU).

Comparing the viable virus collection of the first sampler with the second one enables the determination of absolute BCE of VIVAS. The consideration of viability losses accurately assesses VIVAS's efficiency in capturing viable viruses from sampled air, ultimately enhancing our comprehension of VIVAS's capabilities and limitations in infectious virus sampling for environmental monitoring. The next phase of the study is to test its BCE as a function of low and high aerosol concentrations. This data-driven
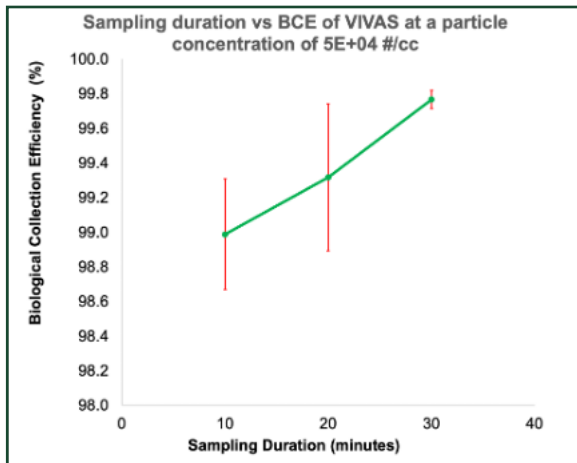
Figure 3. Shows the BCE results of triplicate samples as a function of time. ANOVA reported a significant difference (p=0.00016) in BCE based on sampling durations.

approach facilitates informed decision-making regarding sampling protocols and experimental design, ultimately improving our understanding of VIVAS in capturing viable viruses.

Future research can further validate the performance of VIVAS under realistic environmental conditions and in diverse settings where airborne virus transmission occurs. Field studies conducted in healthcare facilities, public transportation systems, or other high-risk environments. Investigate the BCE of VIVAS for capturing a wide range of virus types, including enveloped and non-enveloped viruses, respiratory viruses, and emerging pathogens. By testing VIVAS with diverse virus strains and species, researchers can assess its versatility and applicability for various surveillance and research purposes.

References

[1] Pan et al. (2016), Journal of Applied Microbiology, 120(3), 805-815.

[2] Hogan et al. (2005), Journal of Applied Microbiology, 99(6), pp.1422-1434

[3] Wu CY, Biswas P. (1998). Aerosol science and technology. 1;28(1):1-20.

Survey of Active Galactic Nuclei in COMAP Observation Regions

Allyson Hudak (Class of 2025)
Major: Dual Major Physics & Chemistry
Principal Investigator: Dr. Joshua Gundersen
Department: Physics

The CO Mapping Array Project (COMAP) employs line intensity mapping (LIM) of carbon monoxide (CO) emissions to efficiently investigate the distribution and evolution of matter over large observation regions and cosmic timescales [1]. LIM sensitivity increases with continued COMAP surveys, but can be enhanced by cross-correlating traditional surveys of active galactic nuclei (AGN) with the COMAP observations. Previous COMAP stacking analyses have been performed with the eBOSS AGN catalog, adding 243 sources to cross-correlate [2] We aim to further increase the number of AGN used in the stacking analysis using University of Miami's AGN Database (AGN-DB) [3], containing over 100 concatenated AGN catalogs.

Traditional galaxy surveys rely on measuring an object's position (in terms of its right ascension and declination) and an object's redshift – an astronomical proxy for distance. This is an inefficient process when investigating the large-scale distribution of mass throughout the universe. COMAP instead measures the aggregate emissions of CO, an abundant molecule in the universe acting as a tracer for overall matter distribution. In its novice years of observation, the Pathfinder instrument used for detection and mapping boasts low levels of sensitivity. AGN are highly luminous sources, and are expected to correlate with COMAP measurements tracing matter distribution. Using this, COMAP intends to enhance its own measurements by stacking the positions of traditionally surveyed AGN onto the Pathfinder observation fields. This has the potential to either reduce the current upper limit on CO emission, or yield a detection for the project. Currently, the stacking analysis includes only sources documented in the eBOSS quasar catalog [2]. This study aims to identify additional relevant sources for addition to the stacking analysis, searching AGN-DB for unique sources matching the parameters of the COMAP project.

AGN eligible for the stacking analysis must overlap with the COMAP observation regions (Figure 1), redshift regime of (2.4-3.4), and must not be duplicates of eBOSS sources already considered in the stack. Additionally, AGN-DB contains several duplicate sources internally as they repeat across different catalogs. The initial data sets were queried from AGN-DB with the help of Jack Hu, a graduate student involved in the development of the database. The COMAP observation regions are centered at the coordinates displayed in Table 1, however, their irregularly shaped perimeters require each to be traced by hand. To accomplish this, the AGN-DB sources were plotted on TOPCAT [4] and overlayed with the eBOSS sources to provide a tracing guide (Figure 1). A polygon shaped subset was then drawn following the outermost eBOSS sources, generating the proper COMAP region shape (Figure 2).

Table 1: The center coordinates of the 2°x2° COMAP observation regions and the number of eBOSS sources contained.

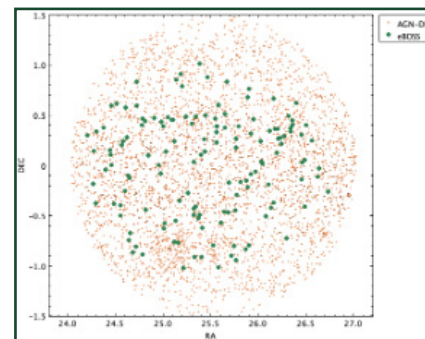|	R.A	Dec	eBOSS Sources
Region 1	25.50 °	0.00 °	140
Region 2	170.00 °	52.50 °	50
Region 3	226.00 °	55.0 °	53

Figure 1: Region 1 AGN-DB Sources with eBOSS sources overlayed.
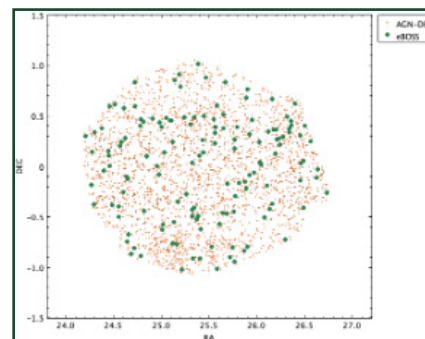

Figure 2: AGN-DB sources contained in region are isolated.

As the eBOSS catalog is contained within AGN-DB, these sources must be removed from the source candidates. Additionally, the internal duplicates of AGN-DB must be removed, particularly those containing lesser-accurate redshift measurements as only candidates with spectroscopic measurements are considered in the stacking analysis. These filters are best accomplished using a combination of TOPCAT's internal match function, assigning identical sources the same ID number, and Python programs to discard those with low-accuracy measurements. The resulting sources must be again filtered based on their redshift measurements using Python, discarding any falling outside of the COMAP range.

Across the three observation regions, the AGN-DB analysis extracted 679 sources within the parameters of the COMAP project (Table 2). Subsequent treatment of each source is dependent on the variety of its redshift measurement.

Table 2: Summary of unique sources extracted from AGN-DB.

	Region 1	Region 2	Region 3
Spectroscopic Redshift	21	12	6
Photometric Redshift	125	75	121
Photo Points	113	93	113
Total	259	180	240

AGN-DB contained 39 unique spectroscopic sources in this category eligible for addition to the COMAP stack. The majority of sources found in this analysis, however, contained either photometric redshift measurements, or none at all in the case of photo points. While these sources are not immediately eligible for the stacking analysis, subsequent treatment of these sources may permit their addition in the future. For the 321 extracted sources containing photometric measurements, we intend to measure their spectroscopic redshift through observation at the Keck Observatory. For this, we are preparing a proposal for observation time in the February-July 2025 semester. Once spectroscopic measurements are acquired, these sources may also be proposed for addition to the stack. The 319 extracted photo points require much more extensive treatment, however, as they must first be analyzed for photometric redshift prior to further observation for spectroscopic measurements. This can be accomplished through spectral energy distribution (SED) fitting, in which the spectral energy distributions of these galaxies are fit to spectral models in order to derive physical properties such as redshift [5]. We plan to use CIGALE, a python code used for SED fitting, to derive the photometric redshift measurements of the photo points. After this process, these sources will also be eligible for spectroscopic redshift observations.Following such treatment, we expect to obtain many additional sources for addition to the COMAP stacking analysis.

References:

[1] Kieran A. Cleary, Et al. COMAP early science. i. overview. The Astrophysical Journal, 933(2):182, jul 2022. ISSN 1538-4357. doi: 10.3847/1538-4357/ac63cc. URL http://dx.doi.org/10.3847/1538-4357/ac63cc.

[2] Delaney A. Dunne, Kieran A. Cleary, Et al. COMAP early science: Viii. a joint stacking analysis with eboss quasars, 2024.

[3]Peca, A. et al., in preparation, 2024

[4] M. B. Taylor. TOPCAT & STIL: Starlink Table/VOTable Processing Software. In P. Shopbell, M. Britton, and R. Ebert, editors, Astronomical Data Analysis Software and Systems XIV, volume 347 of Astronomical Society of the Pacific Conference Series, page 29, December 2005.

[5] Camilla Pacifici, Et al. The art of measuring physical parameter in galaxies: A critical assessment of spectral energy distribution fitting techniques. The Astrophysical Journal, 944(2):141, February 2023. ISSN 1538-4357. doi: 10.3847/1538-4357/acacff.

Axon Regeneration: Assessing Membrane Fluidity Dynamics Through Phosphatidylserine Decarboxylase Using C-Laurdan Dye

Sofia Yarosh (Class of 2026)
Major: Health Science
Principal Investigator: Sanjoy Bhattacharya, Ph.D
Department: Bascom Palmer Eye Institute and Miami Integrative Metabolomics Research Center

This research aims to utilize C-Laurdan dye as a tool to assess membrane fluidity changes resulting from the modulation of phosphatidylserine decarboxylase (PSD) expression levels. By employing knockdown and overexpression techniques, we seek to examine the role of PSD in regulating membrane fluidity and its implications in ophthalmic axon regeneration.

Mitochondrial lipid metabolism plays a crucial role in maintaining cellular homeostasis, energy production, and signaling pathways. The endoplasmic reticulum is a major source of lipids for other cellular structures that either lack the ability to produce their own lipids or have a limited capacity to do so. The exchange and transportation of lipids among organelles depend on specialized carrier proteins, membrane contact sites, tethered complexes, and/or vesicle movement. These mechanisms play a crucial role in maintaining cell structure and viability, contributing significantly to membrane dynamics1. The fluidity of membranes significantly influences how quickly lipids and transmembrane proteins diffuse through them2. Phosphatidylserine decarboxylase (PSD) is a key enzyme involved in this process, catalyzing the formation of phosphatidylethanolamine (PtdEtn) by decarboxylation of phosphatidylserine (PtdSer)3. The lipids produced by PSD are essential for various cellular functions and can be transported to other cellular compartments.

The composition of the acyl chains in membrane lipids is a major factor in determining membrane fluidity[4]. The lipids produced by PSD contain are highly polyunsaturated, which contributes to greater membrane fluidity, elasticity, and flexibility. This unsaturation also leads to a decrease in membrane thickness and the orderliness of its structure.

Both the level of unsaturation and the positioning of these lipids within the membrane affect these properties[5]. Saturated acyl chains can be tightly packed together due to their straight structure, whereas the presence of a kink in unsaturated acyl chains prevents such close packing, allowing for more membrane fluidity[4].
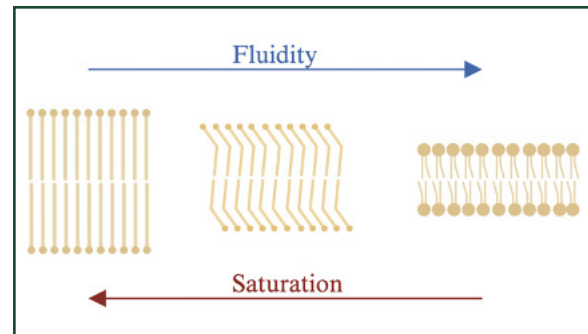

Figure 1. Membrane Fluidity Based on Saturation

To visualize this, PSD transfected cells were treated with C-Laurdan dye, which is sensitive to the polarity of its surrounding environment. Due to its sensitivity, photostability, and high water solubility, C-Laurdan is an extremely useful probe for studying lipid membrane properties, making it increasingly utilized in studies on membrane organization within living cells[6]. Upon excitation, C-Laurdan emits fluorescence with spectral properties dependent on membrane fluidity. Fluorescence microscopy is then utilized to visualize the C-Laurdan labeled cells, and specifically their membranes. Finally, fluorescence intensity will be is then quantified, reflecting changes in membrane fluidity.
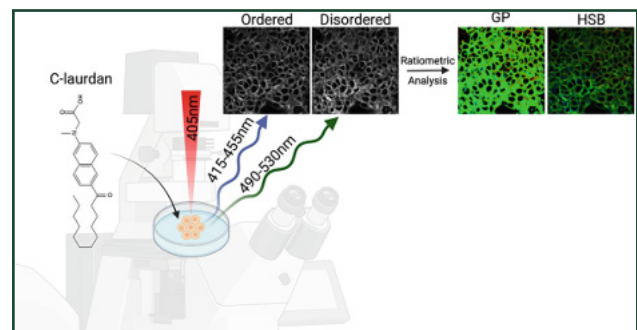

Figure 2. Membrane Order Visualization Using C-Laurdan Dye

The results obtained from C-Laurdan dye staining will provide insights into the changes in membrane fluidity induced by PSD knockdown and overexpression. Decreased PSD expression may lead to reduced levels of highly polyunsaturated lipids, potentially altering membrane fluidity. Alternatively, PSD overexpression may result in an increase in highly polyunsaturated lipids, leading to enhanced membrane fluidity.

Our research highlights the use of C-Laurdan dye as a valuable tool for investigating membrane fluidity dynamics in the context of mitochondrial lipid metabolism. By understanding the role of PSD in affecting membrane fluidity, we can learn more about cellular lipid homeostasis and its implications in eye health and disease.

In the context of ophthalmology, our research focuses on investigating the potential involvement of lipids in axon regeneration, particularly examining the role of PSD-derived phosphatidylethanolamine (PE). While the significance of PSD involvement in regeneration remains underexplored, our study indicates an upregulation of PE in glaucomatous optic nerves. By examining the impact of PSD at various expression levels, we gain insights into its influence on both regeneration and membrane fluidity. Understanding membrane fluidity is crucial in the context of ophthalmic diseases, such as glaucoma, where elevated intraocular pressure prompts cells to enhance fluidity as an adaptive response.

References

[1] Flis VV, Daum G. Lipid transport between the endoplasmic reticulum and mitochondria. Cold Spring Harb Perspect Biol. 2013 Jun 1;5(6):a013235. doi: 10.1101/cshperspect.a013235. PMID: 23732475; PMCID: PMC3660828.

[2] Westra M, Gutierrez Y, MacGillavry HD. Contribution of Membrane Lipids to Postsynaptic Protein Organization. Front Synaptic Neurosci. 2021 Nov 23;13:790773. doi: 10.3389/fnsyn.2021.790773. PMID: 34887741; PMCID: PMC8649999.

[3] Schuiki I, Daum G. Phosphatidylserine decarboxylases, key enzymes of lipid metabolism. IUBMB Life. 2009 Feb;61(2):151-62. doi: 10.1002/iub.159. PMID: 19165886.

[4] Westra M, Gutierrez Y, MacGillavry HD. Contribution of Membrane Lipids to Postsynaptic Protein Organization. Front Synaptic Neurosci. 2021 Nov 23;13:790773. doi: 10.3389/fnsyn.2021.790773. PMID: 34887741; PMCID: PMC8649999.

[5] Rim Baccouch, Yarong Shi, Emilie Vernay, Marion Mathelié-Guinlet, Nada Taib-Maamar, et al.. The impact of lipid polyunsaturation on the physical and mechanical properties of lipid membranes. Biochimica et Biophysica Acta:Biomembranes, 2023, 1865 (2), pp.184084 ff10.1016/j.bbamem.2022.184084ff. Ffhal-03864167f

[6] Dodes Traian MM, Flecha FLG, Levi V. Imaging lipid lateral organization in membranes with C-laurdan in a confocal microscope. J Lipid Res. 2012 Mar;53(3):609-616. doi: 10.1194/jlr.D021311. Epub 2011 Dec 19. PMID: 22184757; PMCID: PMC3276485.

[Figure 2] Meehan SD, Hayter C, Bhattacharya SK. C-Laurdan: Membrane Order Visualization of HEK293t Cells by Confocal Microscopy. Methods Mol Biol. 2023;2625:353-364. doi: 10.1007/978-1-0716-2966-6_30. PMID: 36653657.